Structural basis of hepatocyte growth factor/scatter factor and MET signalling

Ermanno Gherardi*†, Sara Sandin‡, Maxim V. Petoukhov§¶, John Finch‖, Mark E. Youles*, Lars-Göran Öfverstedt‡, Ricardo N. Miguel**, Tom L. Blundell**, George F. Vande Woude††, Ulf Skoglund‡, and Dmitri I. Svergun§¶

*Medical Research Council Centre and ‖Laboratory of Molecular Biology, Hills Road, Cambridge CB2 2QH, United Kingdom; ‡Department of Cell and Molecular Biology, Medical Nobel Institute, Karolinska Institutet, Box 285, 171 77 Stockholm, Sweden; §European Molecular Biology Laboratory, Hamburg Outstation, Notkestrasse 85, D-22603 Hamburg, Germany; ¶Institute of Crystallography, Russian Academy of Sciences, Leninsky Prospect 59, Moscow 117333, Russia; **Department of Biochemistry, University of Cambridge, Tennis Court Road, Cambridge CB2 1GA, United Kingdom; and ††Van Andel Research Institute, 333 Bostwick Avenue Northeast, Grand Rapids, MI 49503

Edited by Joseph Schlessinger, Yale University School of Medicine, New Haven, CT, and approved January 10, 2006 (received for review October 15, 2005)

The polypeptide growth factor, hepatocyte growth factor/scatter factor (HGF/SF), shares the multidomain structure and proteolytic mechanism of activation of plasminogen and other complex serine proteinases. HGF/SF, however, has no enzymatic activity. Instead, it controls the growth, morphogenesis, or migration of epithelial, endothelial, and muscle progenitor cells through the receptor tyrosine kinase MET. Using small-angle x-ray scattering and cryo-electron microscopy, we show that conversion of pro(single-chain)-HGF/SF into the active two-chain form is associated with a major structural transition from a compact, closed conformation to an elongated, open one. We also report the structure of a complex between two-chain HGF/SF and the MET ectodomain (MET928) with 1:1 stoichiometry in which the N-terminal and first kringle domain of HGF/SF contact the face of the seven-blade β-propeller domain of MET harboring the loops connecting the β-strands b–c and d–a, whereas the C-terminal serine proteinase homology domain binds the opposite "b" face. Finally, we describe a complex with 2:2 stoichiometry between two-chain HGF/SF and a truncated form of the MET ectodomain (MET567), which is assembled around the dimerization interface seen in the crystal structure of the NK1 fragment of HGF/SF and displays the features of a functional, signaling unit. The study shows how the proteolytic mechanism of activation of the complex proteinases has been adapted to cell signaling in vertebrate organisms, offers a description of monomeric and dimeric ligand-receptor complexes, and provides a foundation to the structural basis of HGF/SF-MET signaling.

cell signaling | plasminogen | serine proteinases | kringle | x-ray scattering

Hepatocyte growth factor/scatter factor (HGF/SF) (1–6) are vertebrate-specific polypeptide growth factors with a domain structure related to that of plasminogen (7). Interest in HGF/SF and its receptor MET (8) stems from unique biological roles in embryogenesis (9–11), tissue regeneration (12, 13), and cancer (14). These activities have led to a strong interest in the structure of the molecules as this knowledge may underpin the development of MET-based therapeutics.

HGF/SF consists of six domains: an N-terminal domain (n), four copies of the kringle domain (k1–k4), and a C-terminal domain (sp) structurally related to the catalytic domain of serine proteinases (Fig. 1*A*). The factor is synthesized as a precursor protein (pro- or single-chain HGF/SF) and is proteolytically processed to a two-chain form by cleavage of the linker connecting the k4 and sp domains (Fig. 1 *A* and *B*). Single-chain HGF/SF binds MET (15, 16) but is unable to induce biological responses, for example, dispersion of MDCK cell colonies, even at concentrations 100-fold higher than two-chain HGF/SF (Fig. 1 *C–E*).

MET is also synthesized as a single-chain precursor that is cleaved by furin yielding an N-terminal α-chain and a C-terminal β-chain. The MET ectodomain consists of two moieties: the large, N-terminal sema domain, which is responsible for ligand binding and adopts a β-propeller fold, and a stalk structure, which consists of four copies of Ig-like domains (ig) (15) (Fig. 1 *A* and *B*). The sema domain and the stalk structure are joined by a small cystine-rich domain (cr) (Fig. 1*A*).

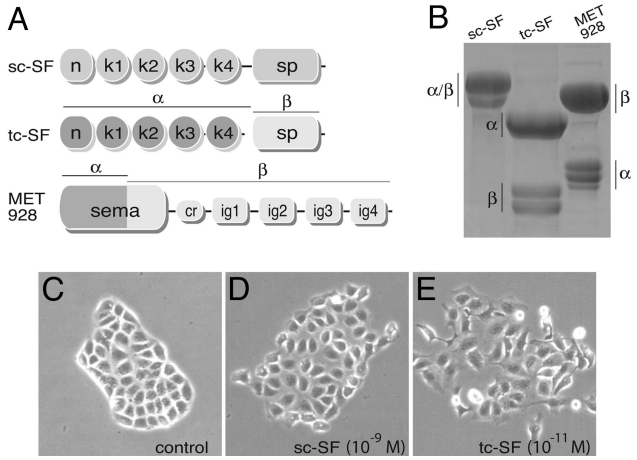

Fig. 1. Domain structure and biological activity of the three main proteins used in this study. (*A*) Domain structure. (*B*) SDS/PAGE under reducing conditions. (*C–E*) Typical appearance of colonies of MDCK cells under standard culture conditions (*C*) or after addition of single-chain (*D*) or two-chain (*E*) HGF/SF at the concentrations indicated. sc-SF, single HGF/SF; tc-SF, two-chain HGF/SF.

The structural basis of the conversion of single-chain to two-chain HGF/SF and MET activation by two-chain HGF/SF are unknown. Several nuclear magnetic resonance and crystal structures of HGF/SF fragments corresponding to the n domain (17), the n and k1 domains (nk1) (18–20), and the sp domain (21), and a crystal structure of the sema and cr domains of MET in complex with the sp domain of HGF/SF (22) have provided important insights but failed to show the interdomain interactions and the relevant changes which underlie biological activity.

The objective of this study is to define structures, by cryo-electron microscopy (cryo-EM) and small-angle x-ray scattering (SAXS), for single-chain and two-chain HGF/SF, the MET ectodomain, and their complexes. Unlike x-ray crystallography and nuclear magnetic resonance, cryo-EM and SAXS can pro-

Conflict of interest statement: No conflicts declared.

This paper was submitted directly (Track II) to the PNAS office.

Abbreviations: CET, cryo-electron tomography; EM, electron microscopy; HGF/SF, hepatocyte growth factor/scatter factor; SAXS, small-angle x-ray scattering; MM, molecular mass.

Data deposition: The atomic coordinates of 3D models of kringles 2, 3, and 4 of HGF/SF and ig2–ig4 of MET have been deposited in the Protein Data Bank, www.pdb.org (PDB ID codes 2CED, 2CEE, 2CEG, and 2CEW).

†To whom correspondence should be addressed. E-mail: egherard@mrc-lmb.cam.ac.uk.

vide critical information on the overall architecture of large and flexible multidomain proteins. For 3D reconstruction of EM preparations, we have used cryo-electron tomography (CET), a method recently and successfully used in protein structure (23) as a result of the development of effective reconstruction and denoising procedures (24). CET offers major advantages over "single particle reconstruction" in cases, such as HGF/SF and MET, in which the proteins under study display structural heterogeneity (see *Results*). Using novel *ab initio* and rigid body modeling methods (25), 3D structures were also, and independently, reconstructed by SAXS, a method that yields truly averaged solution structures over $\approx 10^{15}$ molecules in the illuminated volume. The structures obtained by cryo-EM and SAXS are reported here.

Results

Single-Chain and Two-Chain HGF/SF. The binding affinity of single-chain HGF/SF for MET is high ($K_d \approx 10^{-9}$ M) (16, 26). Why does single-chain HGF/SF fail to activate MET? Under transmission EM, the structures of single-chain and two-chain HGF/SF stained with uranyl acetate differed markedly. The majority of single-chain particles appeared as ring-shaped, closed structures in which the larger sp domain makes contact with the α chain (Fig. 2*A*), and only a few particles displayed an elongated, open conformation (data not shown). In contrast, two-chain HGF/SF, consistently appeared as an elongated molecule (Fig. 2*B*).

Single-chain HGF/SF particles reconstructed by CET[‡‡] ($\approx 130 \times 125 \times 85$ Å) consisted of two distinct moieties, shaped as a rod and a cone and folded against each other (Fig. 2*C*). The volume, shape, and dimensions of the two substructures suggested that the rod contains domains n to k3 (nk3) and that the cone contains the k4 and sp domains, as confirmed by the fact that the available crystal structure of a fragment of thrombin (27) (Fig. 2*G*) corresponding to the k4-sp fragment of HGF/SF could be readily accommodated into the electron density of the cone (Fig. 2*E*). Thus, the short 7-aa linker between k3 and k4, and not the long linker between k4 and sp, acts as a primary molecular hinge in HGF/SF. Unlike single-chain HGF/SF, the majority of two-chain particles reconstructed by CET had an extended structure similar to the one shown in Fig. 2 *D* and *F* and in agreement with the results of negatively stained EM preparations.

SAXS analysis established that both single-chain and two-chain HGF/SF are monomeric in solution and that the R_g and D_{max} of two-chain HGF/SF are larger than those of single-chain (Table 1). Fig. 2*H* presents the processed x-ray scattering patterns and *ab initio* low resolution bead models by DAMMIN (28). These models and all *ab initio* models (Figs. 2*H*, 3*F*, 4*A*, and 5*B*), fitted neatly the experimental data with $\chi \approx 1.0$. The $p(r)$ functions in Fig. 2*I* demonstrated that, although two-chain HGF/SF is more elongated, the two functions are nearly identical up to distances of ≈ 6 nm, suggesting that the difference between the two proteins is because of the movement of one end of the molecule. Rigid body modeling (29) yielded the solutions in Fig. 2*J*, which converge to a common structure for the nk3 segment and differ by a translation of the sp and, to a lesser extent, the k4 domain. Consequently, the receptor binding sites of the k1 (30) and sp (21, 22) domains, shown as blue and red patches in Fig. 2*J*, are very close to each other in the model of single-chain HGF/SF but become separated by >100 Å in two-chain HGF/SF.

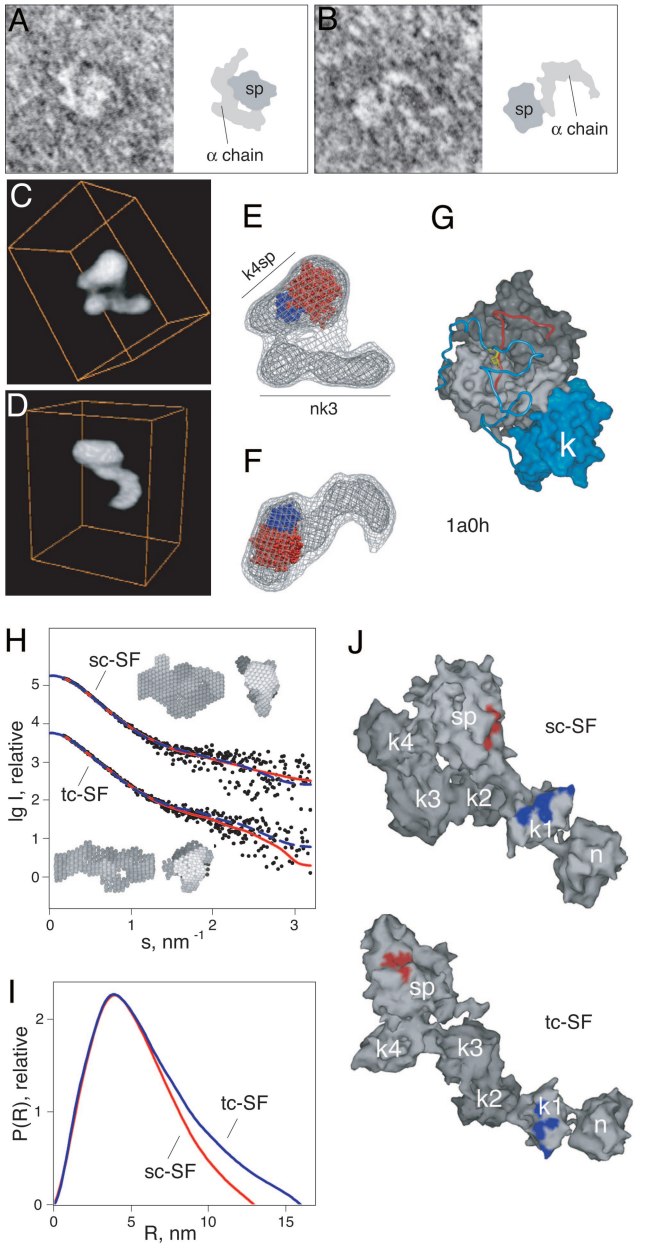

Fig. 2. Structure of single-chain and two-chain HGF/SF. (*A–D*) Appearance of typical particles of single-chain and two-chain HGF/SF after negative staining EM (*A* and *B*) or after 3D reconstruction from CET (*C* and *D*). (*E* and *F*) The docking (45) of the crystal structure of the k2 and sp domains (blue and red, respectively) of bovine thrombin into the electron density maps of the particles shown in *C* and *D*, respectively. (*G*) The crystal structure of the k2-sp fragment of bovine thrombin used for docking (27) (Protein Data Bank accession code 1A0H). The k2 domain is shown in light blue, the N- and C-terminal lobes of the sp domain in dark and pale gray, respectively, and the disulphide bond connecting the α chain and the sp domain is shown in yellow. This disulphide is conserved in HGF/SF and all other members of the kringle-serine proteinase superfamily. SAXS of single-chain and two-chain HGF/SF (*H–J*). The scattering intensities as functions of momentum transfer [$s = 4\pi \sin(\theta)/\lambda$, where 2θ is the scattering angle and $\lambda = 0.15$ nm is the x-ray wavelength] are shown in *H* together with two views, at 90° from each other, of *ab initio* models constructed with DAMMIN (28). Here, and in Figs. 3–5, black dots are experimental data, solid red lines are fits from *ab initio* models, and dashed blue lines are fits from rigid body models. (*I* and *J*) A distance-distribution plot and the rigid body modeling (29) of single-chain and two-chain HGF/SF, respectively. Individual domains are labeled as in Fig. 1, and the area of the k1 (30) and sp (21, 22) domains involved in MET binding are shown in blue and red, respectively. Images in *G–J* were generated with SPOCK. sc-SF, single-chain HGF/SF; tc-SF, two-chain HGF/SF.

[‡‡]Movies 1–4, displaying representative 3D reconstructions, are available as supporting information on the PNAS web site.

BIOCHEMISTRY

Table 1. Structural parameters from the SAXS data

Sample	R_g nm	MM, KDa	MM_{mon}, KDa	D_{max}, nm	V_p, nm^3	Oligomerization state and stoichiometry	χ
sc HGF/SF	4.0 ± 0.1	85 ± 13	90	13.0	140	Monomer	1.04
tc HGF/SF	4.6 ± 0.1	108 ± 16	90	16.0	170	Monomer	1.09
MET567H	3.2 ± 0.1	61 ± 9	72	10.0	120	Monomer	1.63
MET928H	4.8 ± 0.1	91 ± 14	118	16.0	190	Monomer	1.18
sc HGF/SF + MET928H	5.3 ± 0.1	105 ± 18	208	17.0	230	Monomers and 1:1 complex	—
tc HGF/SF + MET928H	6.3 ± 0.1	180 ± 22	208	20.0	370	1:1	1.39
sc HGF/SF + MET567H	5.2 ± 0.1	130 ± 15	162	17.0	250	1:1	0.92
tc HGF/SF + MET567H	6.6 ± 0.1	318 ± 30	162	21.0	550	2:2	1.36 (met) 1.14 (sp) 1.04 (nk1)

R_g, MM, D_{max}, and V_p are calculated from the scattering data. MM_{mon} is computed from the primary structure of monomeric constructs accounting for bound sugars. χ is discrepancy between the experimental data and computed curves from the rigid body models or from the crystallographic model, in the case of MET567 (22). The χ values for the different models of the dimeric complex of two-chain HGF/SF and MET567H are explained in the text.

MET and HGF/SF-MET Complexes. Under negative-staining with uranyl acetate, the MET ectodomain displayed a large globular head corresponding to the sema domain and a long stalk structure (two examples are shown in Fig. 3 *A* and *B*). 3D reconstruction from cryo-EM (Fig. 3 *C* and *D*) showed that the β-propeller domain, shaped as an irregular cylinder of ≈90 × 80 × 65 Å, is arranged with the axis of the blades perpendicular to the major axis of the stalk. The latter differed in individual MET molecules because of flexibility (compare, for example, Fig. 3 C and *D*). The available crystal structure (22) or 3D models (15) of the MET sema, cr, and ig1 domains could be docked accurately into the EM density maps (Fig. 3*E*).

SAXS analysis confirmed that the MET ectodomain is monomeric in solution (Table 1 and Fig. 3 *F* and *G*). The *ab initio* model (Fig. 3*F*) suggested an anisometric arrangement of the domains within the molecule, and the rigid body model (Fig. 3*G*) confirmed the orientation of the β-propeller domain described in Fig. 3 *C* and *D*.

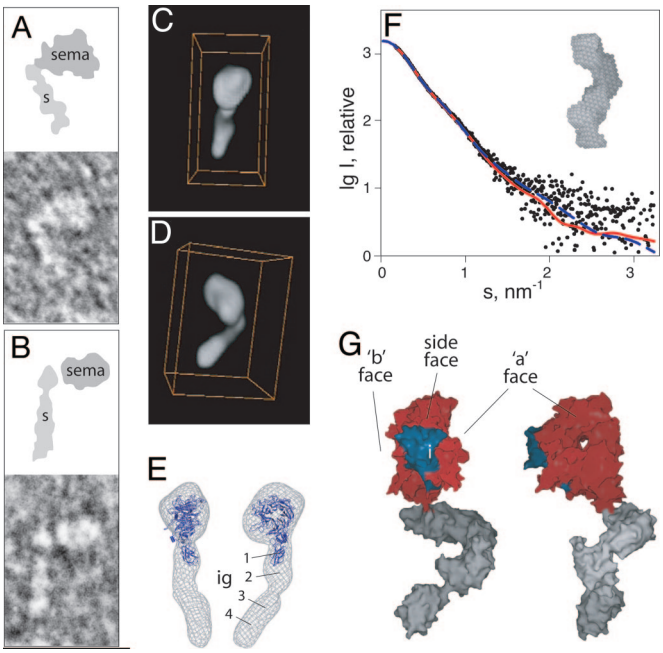

Fig. 3. Structure of the MET ectodomain. (*A–D*) Appearance of MET928 after negative staining EM (*A* and *B*) or 3D reconstruction from CET (*C* and *D*). (*E*) The docking of the three N-terminal domains of MET (sema, cr, and ig1) into the electron density map of the MET particle shown in *C*. (*F* and *G*) SAXS of the MET ectodomain. The scattering curve and an *ab initio* model (28) are shown in *F*; rigid body modeling (29) is shown in *G* (stalk in gray and β-propeller domain in red, except for the insertion in blade 5, which is shown in blue). sc-SF, single HGF/SF; tc-SF, two-chain HGF/SF.

SAXS experiments revealed a different behavior for the binary complexes formed with equimolar ratios of single-chain or two-chain HGF/SF and MET928 (Table 1). Single-chain HGF/SF yielded a mixture of free ligand, receptor, and complex and was not investigated further. In contrast, two-chain HGF/SF and MET928 yielded a monodisperse complex with 1:1 stoichiometry (Table 1 and Fig. 4 *A* and *B*). Comparison of the *ab initio* models demonstrated that the conformations of free and complexed MET928 are similar. Rigid body modeling was next performed to (*i*) simultaneously fit the two experimental curves from free and complexed MET928 by the scattering curves calculated for the appropriate domain subsets and (*ii*) enable contacts between the k1 (30) and sp domains (22) of HGF/SF and MET to be made. The solution obtained by using the above restraints (Fig. 4*B*) is compatible with the *ab initio* shape and shows that (*i*) all of the contacts between two-chain HGF/SF and MET involve the β-propeller domain, (*ii*) the n and k1 domains bind the face of the β-propeller harboring the loops connecting β-strands d–a and b–c[§§], and (*iii*) domains k2–k3 cross the side face of the β-propeller leaving k4 on top of the sp domain.

The 1:1 binary complex formed by two-chain HGF/SF and MET928 was also reconstructed from cryo-EM images (Fig. 4 *C–E* and *F–H*; the latter after low pass filtering at 20 Å). The extra density because of the binding of two-chain HGF/SF to MET928 was readily attributable and consists of a large volume packing against the side face of the β-propeller (Fig. 4*F*), a second one on the "b" face in the area in which the sp binds MET in the crystal structure (22) (Fig. 4*G*), and a third one on the "a" face (Fig. 4*H*). These results can be interpreted with the n and k1 domains of HGF/SF binding the "a" face, the k2–k4 domains being arranged in line along the side surface, and the sp domain binding the "b" face. To bind MET in this manner, the polypeptide chain of two-chain HGF/SF makes two sharp turns: a first one between the k1 and k2 domains and a second between k4 and sp. The 3D EM reconstruction of the complex between two-chain HGF/SF and MET928 was analyzed further by docking the SAXS rigid body model into the EM density envelope. The results (Fig. 4 *I–K*) produced a remarkable fit, at the level of resolution available, and confirmed the mode of binding described in Fig. 4*B*.

[§§]In work with other β-propellers, this surface has often been designated as the "top face," but, because of the vertical arrangement of the MET β-propeller, we call this face "a" and the opposite one "b" to avoid ambiguity (Fig. 3*G*).

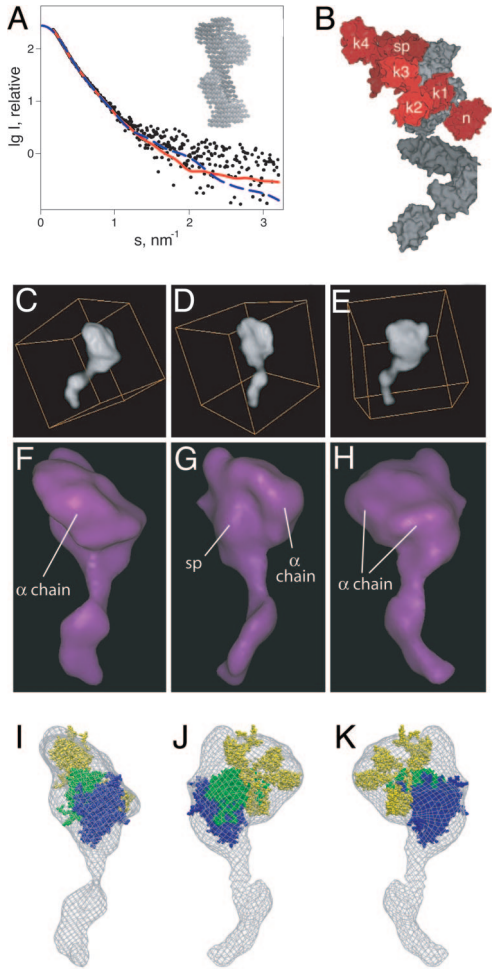

Fig. 4. The 1:1 complex formed by two-chain HGF/SF and MET928. (*A* and *B*) SAXS of the two-chain HGF/SF-MET928 complex. (*A*) Scattering curve and *ab initio* model (28). (*B*) Rigid body model (29) (MET928 in gray, two-chain HGF/SF in red). (*C–K*) CET of the two-chain HGF/SF-MET928 complex. (*C–E*) Three views of a typical 3D reconstruction. (*F–H*) Corresponding images after low pass filtering. (*I–K*) Docking of the SAXS model of the two-chain HGF/SF-MET928 complex into the EM density envelope (MET β-propeller in blue; sp domain of HGF/SF in green; other HGF/SF domains in yellow); sc-SF, single-chain HGF/SF; tc-SF, two-chain HGF/SF.

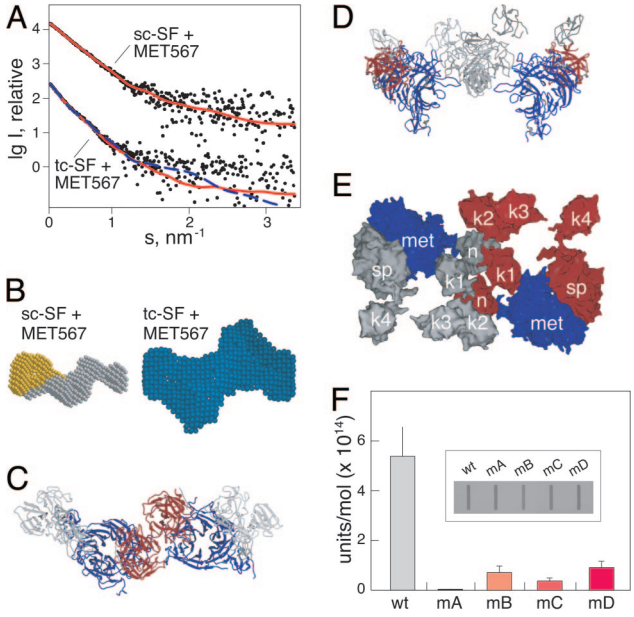

Fig. 5. The complexes formed by single-chain and two-chain HGF/SF with MET567. (*A* and *B*) SAXS of the complexes formed by single-chain and two-chain HGF/SF with MET567. (*A*) Scattering curves. (*B*) *Ab initio* models. In the *ab initio* model of the complex with single-chain HGF/SF (generated with MONSA (28), MET567 is shown in yellow, and single-chain HGF/SF is shown in gray. The *ab initio* model of the complex of two-chain HGF/SF with MET567 was generated with DAMMIN (28). (*C–E*) Rigid body models of the 2:2 complex between two-chain HGF/SF and MET567 in which the dimerization interface is provided by the sp domain (*C*) or the n and k1 domains (*D* and *E*). In *C* and *D*, MET is shown in blue, the sp domain in red, and other HGF/SF domains in gray. In *E*, MET is shown in blue and the two different molecules of two-chain HGF/SF are shown in red and gray, respectively. *C–E* were generated with SPOCK. (*F*) Expression and biological activity of wild-type and mutant HGF/SF proteins. Wild-type HGF/SF and four mutants (mutA, E159A:S161A:E195A:R197A:Y198A; mutB, F82A:T83A:K85A; mutC, D123A:N127A; and mutD, V140A:I142A) were expressed transiently in Neuro2A cells. Protein levels were monitored by slot blot (*Inset*) and quantitated by a sandwich antibody assay. Biological activity was measured on MDCK cells (1, 4), and results were expressed as specific activity. Values are mean and standard deviation from triplicate transfections, and each mutant has been tested in at least three separate experiments. sc-SF, single-chain HGF/SF; tc-SF, two-chain HGF/SF.

The Elusive MET Dimer. Although earlier studies by analytical ultracentrifugation (15) and the present SAXS and EM studies (Fig. 4) failed to detect dimeric complexes between HGF/SF and MET928, studies with a shorter MET fragment (MET567) offered the first clues to MET dimerization and are described below.

MET567, a construct which contains the sema and cr domains of MET (Fig. 1*A*) was monomeric in solution (Table 1), and the scattering curve calculated from the available atomic coordinates (22) agreed with the experimental data (data not shown). Single-chain HGF/SF and MET567 formed a stable complex with 1:1 stoichiometry (Fig. 5*A* and Table 1). The *ab initio* program MONSA (28) was used to simultaneously fit three data sets (from single-chain HGF/SF, MET567, and their complex) by a multiphase bead model, and the results indicated that only one end of single-chain HGF/SF binds MET567 (Fig. 5*B*, single-chain HGF/SF in gray and MET567 in orange). In contrast, the scattering pattern (Fig. 5*A*) and structural parameters (Table 1) from equimolar mixtures of two-chain HGF/SF and MET567 demonstrated a complex with 2:2 stoichiometry (Fig. 5 *A* and *B*).

Because receptor dimerization can occur as a result of either ligand (31, 32) or receptor contacts (33, 34), we studied the ability of two-chain HGF/SF or MET to dimerize in the presence of cross-linking reagents. Dimer formation was readily seen in the presence of cross-linker and, in the case of two-chain HGF/SF, higher order oligomers were also present (Fig. 6, which is published as supporting information on the PNAS web site). The cross-linking experiments, therefore, could not identify or exclude, unequivocally, two-chain HGF/SF or MET as the dimerizing species.

We extracted the region corresponding to two-chain HGF/SF and MET567 from the model of the 1:1 complex shown in Fig. 4*B* and generated several models of the dimeric complex assuming a 2-fold axis around the MET or sp (22) or nk1 (18–20) domains. The dimer constructed through the MET interface produced a good fit to the experimental data ($\chi = 1.36$) but with some systematic deviations (data not shown). Two possible models based on the sp interface yielded poor fits to the data ($\chi = 3.4$ and 3.3). Refinement of one of them improved the fit significantly ($\chi = 1.14$) but required an arrangement of the HGF/SF domains different from that of the initial 1:1 complex (Fig. 5*C*). Strikingly, a model based on the dimerization interface seen in the crystal structure of nk1 (18–20) neatly fitted the

experimental data without refinement ($\chi = 1.04$) and yielded two receptor molecules arranged in parallel as expected for the physiological MET dimer (Fig. 5 *D* and *E*).

To gain further insights into the putative nk1 mode of dimerization, a k1 mutant (mutA: E159A:S161A:E195A:R197A:Y198A) deficient in MET binding (30) and three mutants, corresponding to clusters of amino acids in the n domain (mutB: F82A:T83A:K85A), the n-k1 linker (D123A:N127A), and the k1 domain (V140A:I142A), involved in dimer formation (18–20) were produced (see Fig. 7, which is published as supporting information on the PNAS web site). Wild-type HGF/SF and the four mutants were expressed in COS7 and Neuro2a cells by transient transfection and compared for protein levels (Fig. 5*F Inset*) and biological activity in MDCK colony scatter assays (4). As expected, the activity of the binding-deficient mutA protein was barely detectable (Fig. 5*F*). Interestingly, although, the activity of the three mutants at the nk1 dimerization interface was also considerably reduced (8.6%, 6.7%, and 16.2% of wild-type HGF/SF for mutB, mutC, and mutD, respectively) (Fig. 5*F*). These results strongly suggest that a dimerization interface similar to the one seen in the crystal structures of nk1 (18–20) may be responsible for HGF/SF-mediated dimerization of MET on the cell surface.

Discussion

There are important structural similarities, as well as differences, between the proenzyme plasminogen and single-chain HGF/SF. Both proteins appear to be in equilibrium between a prevailing compact (closed) conformation and an elongated (open) one. Under negatively stained EM, the compact form of plasminogen appears to have a spiral structure (35) stabilized by contacts between the n domain and k5 (36). The closed conformation of single-chain HGF/SF is not spiral but is produced by the k4-sp domains folding back onto the N-terminal part of the molecule; the intramolecular contacts that stabilize the closed conformation of HGF/SF are also different from plasminogen, involving the sp domain and probably k2 (Fig. 2 *C* and *E*). The open form plasminogen is a better substrate for activation (37), and, given that plasminogen activators can activate single-chain HGF/SF, preferential cleavage of the open form may also occur with single-chain HGF/SF. As for receptor binding, the closed form of single-chain HGF/SF is clearly unable to bind MET with both the nk1 and sp domains because of steric hindrance (Fig. 2 *C* and *J*). It is also conceivable that only the open form of single-chain HGF/SF binds MET and that, in the presence of the receptor, the equilibrium shifts toward the open form, an interpretation in agreement with the shape of the 1:1 complex formed by single-chain HGF/SF and MET567 (Fig. 5*B*). In essence, the structural theme underlying the regulation of plasminogen and other complex serine proteinases is conserved in HGF/SF, although critical differences have emerged from this study concerning the architecture of the two proteins and the interdomain interactions responsible for the inactive state.

The readiness by which two-chain HGF/SF forms a 2:2 complex with MET567 was unexpected. An obvious function of the MET stalk is in transducing the HGF/SF signal, but the present study suggests that the stalk may also hold the β-propeller domain in a conformation that enables a 1:1 ligand-receptor complex but restrains dimerization. Dimerization of the 1:1 complex may occur transiently in membrane microdomains in which receptor particles are clustered at high density (38). It may also be facilitated by heparan sulfate proteoglycans (15), the juxtamembrane domain of MET, or coreceptor proteins, although the work with MET567 establish that none of these factors is an absolute prerequisite for dimerization (Table 1 and Fig. 5*A*).

The SAXS experiments with MET567 suggested that the n and k1 domains may provide the dimer interface, as seen in the crystal structure of the nk1 (18–20) and initial mutagenesis experiments (Fig. 5*F*) support this interpretation. The nk4 fragment (39) or single-chain HGF/SF may thus fail to yield a 2:2 complex with MET because in nk4 the sp domain is missing and in single-chain HGF/SF the domain is locked in a conformation that only enables low affinity binding (21); lack of binding through the sp domain may destabilize dimerization via the n and k1 domains. As for the proposed role for the sp domain in MET dimerization (22), the results of our study suggest an alternative one, namely in the formation of higher-order signaling complexes. There is biochemical evidence for high-molecular weight HGF/SF-MET complexes on the cell surface (38), and the sp domain may be involved in the assembly of such oligomers through the domain surface opposite to the one involved in MET binding.

In conclusion, we have obtained low-resolution structures of single-chain and two-chain HGF/SF, the MET ectodomain, and their complexes. The models obtained independently by SAXS and cryo-EM are consistent, define the main conformation of the inactive state of single-chain HGF/SF, clarify the mode of binding of two-chain HGF/SF to MET, and suggest that MET dimerization may occur through a ligand interface involving the n and k1 domain, a conclusion supported by initial mutagenesis experiments. The study offers a glimpse of the structural basis of HGF/SF and MET signaling and provides a foundation to the efforts aimed at producing MET antagonists for cancer therapy.

Materials and Methods

Negative-Staining Electron Microscopy. Carbon-coated grids were glow discharged, and the protein solution applied, rinsed with 0.1 M KCl and 2% uranyl acetate, blotted, air dried, and examined in a Philips EM208 microscope (Eindhoven, The Netherlands). Protein samples were in 50 mM Mes/150 mM NaCl, pH 6.7. Only particles in which all protein domains appeared discernible were used for analysis (24 particles of single-chain HGF/SF, 61 particles of two-chain HGF/SF, and 48 particles of MET928; examples of which are given in *Results*).

Cryo-EM. Protein samples (1.6 to 6.9 mg/ml in either 50 mM Mes/150 mM NaCl, pH 6.7 or 50 mM Tris·Cl/150 mM NaCl, pH 7.2) were mixed with a suspension of 10 nm gold particles at a ratio 2:1, vol/vol. Details of subsequent specimen handling and data acquisition have been described (23). The CET method covers a resolution range of 20–100 Å, and the proteins studied here are flexible, hence resolution cannot be determined by a measure of the similarity between two calculated averages. To assess the quality of the CET reconstructions, we have used the atomic structures of individual domains, i.e., the sp domain of HGF/SF and the sema domain of MET (22). The crystal structures fit well into the tomograms and the correlation coefficient at 20-Å resolution ranged from 0.68–0.79, higher than the 0.5 threshold criteria generally used to estimate resolution. The following number of particles were reconstructed, refined, and studied individually for size, geometry, and domain docking: single-chain HGF/SF (193 particles, of which 61 were refined), two-chain HGF/SF (162 particles, of which 55 were refined), MET928 (192 particles, of which 108 were refined), and two-chain HGF/SF-MET928 complex (86 particles, of which 34 were refined).

Small-Angle X-Ray Scattering. Synchrotron SAXS data were collected on the EMBL X33 camera with a linear gas detector (40, 41) on the storage ring DORIS III [Deutsches Elektronen-Synchrotron (DESY), Hamburg, Germany). All samples were measured at several solute concentrations ranging from 1.2 to 9.1 mg/ml in 50 mM Mes/150 mM NaCl, pH 6.7 in the range of momentum transfer $0.15 < s < 3.5$ nm^{-1} and, in several experiments, 5 mM DTT was added to the buffer. The data were

processed by the program PRIMUS (42) by using standard procedures (25) to compute the radius of gyration R_g, excluded (Porod) volume V_p, and maximum dimension D_{max}. The distance distribution function $p(r)$ was computed by using the program GNOM (43). The molecular masses (MM) of the solutes were evaluated by scaling against reference solutions of BSA and further verified by comparison with the excluded particle volume (for globular proteins, V_p in nm^3 is about twice the MM in kDa). Particle shapes at low resolution were reconstructed *ab initio* by the bead-modeling programs DAMMIN and MONSA (28). The scattering amplitudes of the individual subunits were calculated from their atomic coordinates with carbohydrate side chains added to the appropriate asparagines, by using the program CRYSOL (44). Rigid body modeling was performed by the simulated annealing programs BUNCH and SASREF (29) to find optimal spatial configurations of the domains/subunits fitting the scattering data from the complex. In BUNCH, flexible interdomain linkers were represented as chains of dummy residues. For all *ab initio* and rigid body analysis based on SAXS data, multiple runs were performed to verify the stability of the solution.

Other Methods. Recombinant, single-chain, and two-chain HGF/SF were produced in mouse NIH 3T3 fibroblasts and NS0 myeloma cells after stable transfection. For experiments with cells in cultures (Fig. 1), an uncleavable form of single-chain HGF/SF (R494E) was used. Recombinant MET928 and MET567 were expressed and purified as described (15). For cross-linking experiments, aliquots of protein solutions (0.1 mg/ml in 50 mM Na phosphate/150 mM NaCl, pH 7.2) were incubated in the presence of different ratios of bis(sulfosuccinimidyl)suberate (BS^3) (Pierce) for 30 min at room temperature before quenching with 1 μl of 1M Tris·Cl, pH 7.4 and loading onto a 10% SDS/PAGE gel run under nonreducing conditions. For mutagenesis of HGF/SF, a PCR-based method was used, and mutations were confirmed by DNA sequencing. Wild-type and mutant HGF/SF proteins were expressed transiently in COS7 and Neuro2A cells by using Lipofectamine 2000 (Invitrogen), and their concentration in the supernatant was measured by using a sandwich enzyme-linked antibody assay (cat DY294, R & D Systems). MDCK colony scatter assays were carried out as described (1, 4).

E.G. is grateful to Andreas Bohne (Deutsches Krebsforschungszentrum, Heidelberg) for advice on modeling carbohydrate side chains; Hartmut Niemann (German Research Center for Biotechnology, Braunschweig, Germany), Michael Stoker, and members of the laboratory for critical reading of the manuscript; and Lauris Kemp for discussions. Work in E.G.'s laboratory is supported by Medical Research Council Program Grant G9704528. Work in U.S.'s laboratory is supported by grants from the Agouron Institute, the Karolinska Foundation, the Knowledge Foundation, the Swedish Foundation for Strategic Research, and the Swedish Research Council, and by support from European Union Grant PF6 NoE 3D-EM. M.V.P. acknowledges support by a Structural Proteomics in Europe (SPINE) fellowship under the European Union Contract QLG2-CT-2002-00988. E.G. also has a part-time teaching appointment at the University of Pavia, Italy.

1. Gherardi, E., Gray, J., Stoker, M., Perryman, M. & Furlong, R. (1989) *Proc. Natl. Acad. Sci. USA* **86,** 5844–5848.
2. Nakamura, T., Nishizawa, T., Hagiya, M., Seki, T., Shimonishi, M., Sugimura, A., Tashiro, K. & Shimizu, S. (1989) *Nature* **342,** 440–443.
3. Miyazawa, K., Tsubouchi, H., Naka, D., Takahashi, K., Okigaki, M., Arakaki, N., Nakayama, H., Hirono, S., Sakiyama, O., Takahashi, K., *et al.* (1989) *Biochem. Biophys. Res. Commun.* **163,** 967–973.
4. Stoker, M., Gherardi, E., Perryman, M. & Gray, J. (1987) *Nature* **327,** 239–242.
5. Weidner, K. M., Arakaki, N., Hartmann, G., Vandekerckhove, J., Weingart, S., Rieder, H., Fonatsch, C., Tsubouchi, H., Hishida, T., Daikuhara, Y., *et al.* (1991) *Proc. Natl. Acad. Sci. USA* **88,** 7001–7005.
6. Gherardi, E. & Stoker, M. (1990) *Nature* **346,** 228 (lett.).
7. Donate, L. E., Gherardi, E., Srinivasan, N., Sowdhamini, R., Aparicio, S. & Blundell, T. L. (1994) *Protein Sci.* **3,** 2378–2394.
8. Bottaro, D. P., Rubin, J. S., Faletto, D. L., Chan, A. M., Kmiecik, T. E., Vande Woude, G. F. & Aaronson, S. A. (1991) *Science* **251,** 802–804.
9. Schmidt, C., Bladt, F., Goedecke, S., Brinkmann, V., Zschiesche, W., Sharpe, M., Gherardi, E. & Birchmeier, C. (1995) *Nature* **373,** 699–702.
10. Uehara, Y., Minowa, O., Mori, C., Shiota, K., Kuno, J., Noda, T. & Kitamura, N. (1995) *Nature* **373,** 702–705.
11. Bladt, F., Riethmacher, D., Isenmann, S., Aguzzi, A. & Birchmeier, C. (1995) *Nature* **376,** 768–771.
12. Huh, C. G., Factor, V. M., Sanchez, A., Uchida, K., Conner, E. A. & Thorgeirsson, S. S. (2004) *Proc. Natl. Acad. Sci. USA* **101,** 4477–4482.
13. Borowiak, M., Garratt, A. N., Wustefeld, T., Strehle, M., Trautwein, C. & Birchmeier, C. (2004) *Proc. Natl. Acad. Sci. USA* **101,** 10608–10613.
14. Birchmeier, C., Birchmeier, W., Gherardi, E. & Vande Woude, G. F. (2003) *Nat. Rev. Mol. Cell Biol.* **4,** 915–925.
15. Gherardi, E., Youles, M. E., Miguel, R. N., Blundell, T. L., Iamele, L., Gough, J., Bandyopadhyay, A., Hartmann, G. & Butler, P. J. (2003) *Proc. Natl. Acad. Sci. USA* **100,** 12039–12044.
16. Lokker, N. A., Mark, M. R., Luis, E. A., Bennett, G. L., Robbins, K. A., Baker, J. B. & Godowski, P. J. (1992) *EMBO J.* **11,** 2503–2510.
17. Zhou, H., Mazzulla, M. J., Kaufman, J. D., Stahl, S. J., Wingfield, P. T., Rubin, J. S., Bottaro, D. P. & Byrd, R. A. (1998) *Structure* **6,** 109–116.
18. Chirgadze, D. Y., Hepple, J. P., Zhou, H., Byrd, R. A., Blundell, T. L. & Gherardi, E. (1999) *Nat. Struct. Biol.* **6,** 72–79.
19. Watanabe, K., Chirgadze, D. Y., Lietha, D., de Jonge, H., Blundell, T. L. & Gherardi, E. (2002) *J. Mol. Biol.* **319,** 283–288.
20. Ultsch, M., Lokker, N. A., Godowski, P. J. & de Vos, A. M. (1998) *Structure* **6,** 1383–1393.
21. Kirchhofer, D., Yao, X., Peek, M., Eigenbrot, C., Lipari, M. T., Billeci, K. L., Maun, H. R., Moran, P., Santell, L., Wiesmann, C. & Lazarus, R. A. (2004) *J. Biol. Chem.* **279,** 39915–39924.
22. Stamos, J., Lazarus, R. A., Yao, X., Kirchhofer, D. & Wiesmann, C. (2004) *EMBO J.* **23,** 2325–2335.
23. Sandin, S., Öfverstedt, L.-G., Wikstrom, A. C., Wrange, O. & Skoglund, U. (2004) *Structure* (*London*) **12,** 409–415.
24. Skoglund, U., Öfverstedt, L.-G., Burnett, R. M. & Bricogne, G. (1996) *J. Struct. Biol.* **117,** 173–188.
25. Svergun, D. I. & Koch, M. H. J. (2003) *Rep. Prog. Phys.* **66,** 1735–1782.
26. Mazzone, M., Basilico, C., Cavassa, S., Pennacchietti, S., Risio, M., Naldini, L., Comoglio, P. M. & Michieli, P. (2004) *J. Clin. Invest.* **114,** 1418–1432.
27. Martin, P. D., Malkowski, M. G., Box, J., Esmon, C. T. & Edwards, B. F. (1997) *Structure* **5,** 1681–1693.
28. Svergun, D. I. (1999) *Biophys. J.* **76,** 2879–2886.
29. Petoukhov, M. V. & Svergun, D. I. (2005) *Biophys. J.* **89,** 1237–1250.
30. Lokker, N. A., Presta, L. G. & Godowski, P. J. (1994) *Protein Eng.* **7,** 895–903.
31. Pellegrini, L., Burke, D. F., von Delft, F., Mulloy, B. & Blundell, T. L. (2000) *Nature* **407,** 1029–1034.
32. Wiesmann, C., Ultsch, M. H., Bass, S. H. & de Vos, A. M. (1999) *Nature* **401,** 184–188.
33. Garrett, T. P., McKern, N. M., Lou, M., Elleman, T. C., Adams, T. E., Lovrecz, G. O., Zhu, H. J., Walker, F., Frenkel, M. J., Hoyne, P. A., *et al.* (2002) *Cell* **110,** 763–773.
34. Ogiso, H., Ishitani, R., Nureki, O., Fukai, S., Yamanaka, M., Kim, J. H., Saito, K., Sakamoto, A., Inoue, M., Shirouzu, M. & Yokoyama, S. (2002) *Cell* **110,** 775–787.
35. Tranqui, L., Prandini, M. H. & Chapel, A. (1979) *Biol. Cell.* **34,** 39–42.
36. Cockell, C. S., Marshall, J. M., Dawson, K. M., Cederholm-Williams, S. A. & Ponting, C. P. (1998) *Biochem. J.* **333,** 99–105.
37. Markus, G. (1996) *Fibrinolysis* **10,** 75–85.
38. Tsarfaty, I., Rong, S., Resau, J. H., Rulong, S., da Silva, P. P. & Vande Woude, G. F. (1994) *Science* **263,** 98–101.
39. Date, K., Matsumoto, K., Shimura, H., Tanaka, M. & Nakamura, T. (1997) *FEBS Lett.* **420,** 1–6.
40. Koch, M. H. J. & Bordas, J. (1983) *Nucl. Instrum. Methods* **208,** 461–469.
41. Gabriel, A. & Dauvergne, F. (1982) *Nucl. Instrum. Methods* **201,** 223–224.
42. Konarev, P. V., Volkov, V. V., Sokolova, A. V., Koch, M. H. J. & Svergun, D. I. (2003) *J. Appl. Crystallogr.* **36,** 1277–1282.
43. Svergun, D. I. (1992) *J. Appl. Crystallogr.* **25,** 495–503.
44. Svergun, D. I., Barberato, C. & Koch, M. H. J. (1995) *J. Appl. Crystallogr.* **28,** 768–773.
45. Wriggers, W., Milligan, R. A. & McCammon, J. A. (1999) *J. Struct. Biol.* **125,** 185–195.